Protease-Activated Receptor (PAR) 2, but not PAR1, Signaling Promotes the Development of Mammary Adenocarcinoma in Polyoma Middle T Mice

Henri H. Versteeg,[1] Florence Schaffner,[1] Marjolein Kerver,[1] Lesley G. Ellies,[2] Patricia Andrade-Gordon,[4] Barbara M. Mueller,[3] and Wolfram Ruf[1]

[1]Department of Immunology, The Scripps Research Institute; [2]Department of Pathology, University of California at San Diego, La Jolla, California; [3]Sidney Kimmel Cancer Center, San Diego, California; and [4]Johnson & Johnson PRD, Spring House, Pennsylvania

Abstract

The G protein–coupled protease-activated receptors (PAR) are key signaling components for proteases in vascular biology and tumor progression. To address the contributions of PAR1 and PAR2 to breast cancer development, we established cohorts of mouse mammary tumor virus–polyoma middle T (PyMT) PAR1$^{-/-}$ and PAR2$^{-/-}$ mice, considering that the PyMT model recapitulates aspects of human disease. Appearance of palpable tumors, tumor expansion, and metastasis was indistinguishable between wild-type and PAR1$^{-/-}$ mice. PAR1$^{-/-}$ breast cancer cells were no longer responsive to thrombin *in vitro*, excluding compensatory up-regulation of alternative thrombin receptors and indicating that thrombin-PAR1 signaling is dispensable in breast tumor microenvironments. In contrast, palpable tumors and multifocal disease developed slower in PAR2$^{-/-}$ mice, and as a consequence of delayed tumor onset, metastasis was reduced. Analysis of early tumors showed persistence of adenomas with delayed appearance of vascularized adenocarcinomas in PAR2$^{-/-}$ mice. Furthermore, CXCL1 production by early PAR2$^{-/-}$ tumors was reduced. These results are consistent with previous xenograft data that implicated breast cancer PAR2 signaling in the induction of proangiogenic growth factors and chemokines. This study establishes that protease signaling contributes to mammary tumor development and that PAR2, rather than the thrombin receptor PAR1, plays a crucial role in the angiogenic switch. [Cancer Res 2008;68(17):7219–27]

Introduction

Local coagulation activation is a hallmark of cancers and cancer-associated thrombosis and Trousseau's syndrome are frequent complications of advanced cancer and metastatic disease (1). Intriguingly, prolonged thromboprophylaxis reduces cancer incidence (2), indicating that the coagulation pathway also promotes early stages of tumor development. Cancer cell–expressed tissue factor (TF) is the major procoagulant stimulus in cancer (3) and tumor cell TF expression promotes cancer growth in most, but not all, tumor models (4–8).

TF forms a catalytic enzyme complex with coagulation factor VIIa and the TF-VIIa complex typically triggers coagulation and thrombin-dependent fibrin deposition, platelet activation, and other pleiotropic cellular effects mediated by thrombin activation of G protein–coupled protease-activated receptor (PAR) 1. Thrombin also activates PAR4, which is a low-affinity thrombin receptor of importance for platelet activation. Within the tumor microenvironment, thrombin may regulate angiogenesis and tumor progression (9) and thrombin plays pivotal roles in hematogenous metastasis (10). Furthermore, the tumor cell–expressed or host-expressed TF-VIIa complex also signals directly by cleaving PAR2, but not PAR1 (3). On tumor cells, TF-VIIa signaling induces a diverse repertoire of angiogenic regulators and immunomodulatory cytokines (11, 12), which is partially overlapping with thrombin-induced signaling (9). These data and the findings that PAR1 or PAR2 deficiency alone does not impair the growth of transplanted syngeneic tumors or of metastases (13, 14) raise the issue whether direct TF signaling on tumor cells is redundant with other protease signaling pathways in the tumor microenvironment.

Coagulation-inactive cellular pools of TF retain direct cell signaling activity (15) and tumor cells ectopically synthesize the ligand of TF, coagulation factor VIIa (16). Thus, TF-VIIa signaling may predominate before angiogenesis-dependent extravasation of coagulation factors that induce thrombin signaling. Interactions with extracellular matrix proteins may be important in this process because TF-VIIa signaling specifically regulates $\alpha3\beta1$-dependent migration (17), and in cancer cells, TF is constitutively associated with $\alpha3\beta1$ and $\alpha6\beta1$ integrins that control TF-VIIa–mediated PAR2 activation (18). PAR2 signaling can then promote breast cancer motility through interleukin-8 (IL-8) induction and cofilin pathways (12, 19, 20). Importantly, inhibition of TF-integrin association and TF-VIIa-PAR2 signaling, but not of PAR1 cleavage, is sufficient to attenuate the growth of highly aggressive human breast cancer cells in a xenograft model (18).

Xenograft models do not necessarily recapitulate all aspect of spontaneous tumor progression and the relative importance of PAR1 and PAR2 signaling in breast cancer development remains incompletely understood. Thrombin-mediated PAR1 activation does not enhance breast cancer motility (21), but matrix metalloproteinase-1 promotes PAR1-dependent invasion (22). PAR1 signaling has been the focus of several studies and was linked to cancer cell invasion and metastasis (9, 23–26). Overexpression experiments show that PAR1 has oncogenic activity but alone is insufficient to promote the development of aggressive carcinoma (27–29).

To avoid limitations of specific tumor cell lines, we here addressed spontaneous mammary tumor development in PAR1$^{-/-}$ and PAR2$^{-/-}$ mice. We used the mouse model of polyoma middle T (PyMT) oncogene expression under the control of the mouse mammary tumor virus (MMTV) promoter (30), a model that

Note: H.H. Versteeg and F. Schaffner contributed equally to this work.

Requests for reprints: Wolfram Ruf, Department of Immunology, SP258, The Scripps Research Institute, La Jolla, CA 92037. Phone: 858-784-2748; Fax: 858-784-8480; E-mail: ruf@scripps.edu.

doi:10.1158/0008-5472.CAN-08-0419

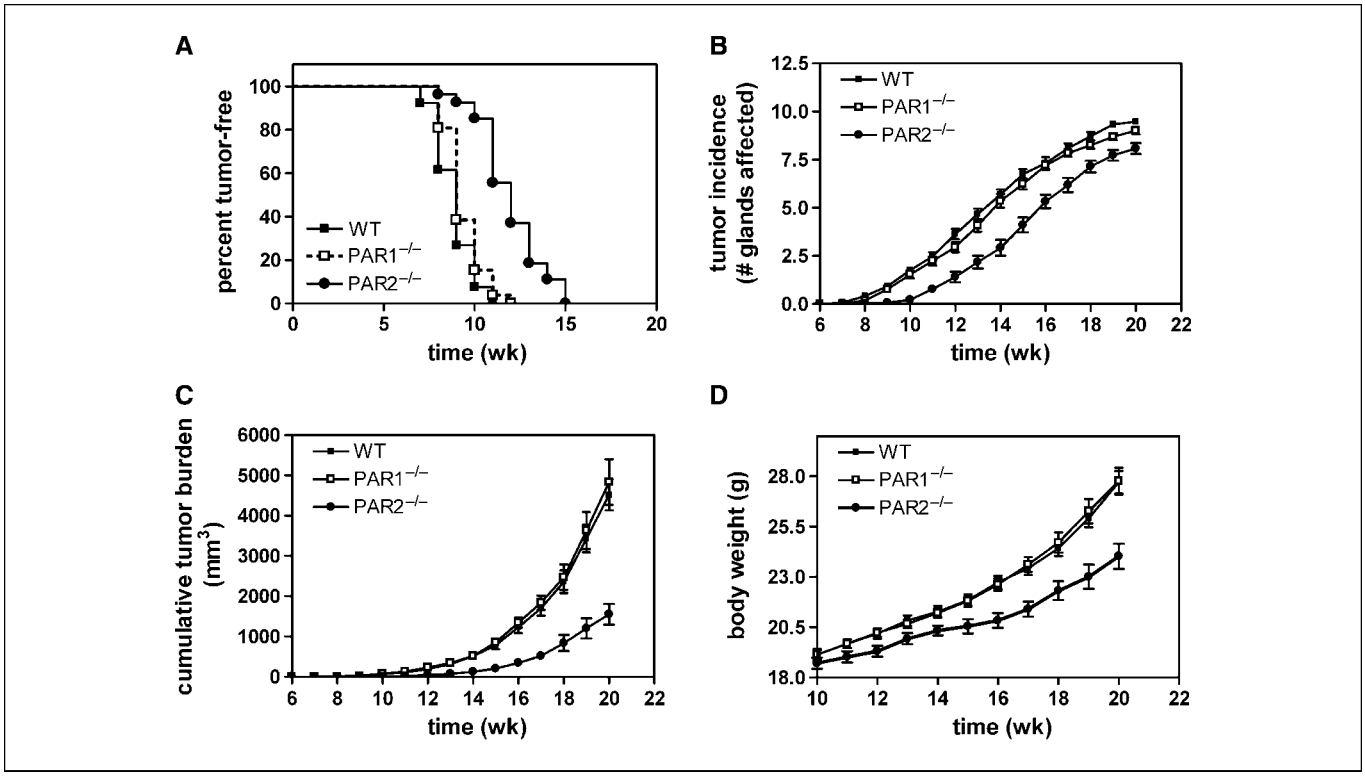

Figure 1. PAR2, but not PAR1, supports spontaneous breast cancer development. *A,* female WT C57BL/6, PAR1$^{-/-}$, or PAR2$^{-/-}$ PyMT mice were examined once per week for the appearance of palpable tumors in either of the mammary glands. The time of tumor-free survival was recorded and plotted for the cohorts of 26 WT, 26 PAR1$^{-/-}$, and 27 PAR2$^{-/-}$ mice. The mean time to tumor appearance was 12 wk (PAR2$^{-/-}$), 8.9 wk (WT), and 9.0 wk (PAR1$^{-/-}$). Delay in tumor appearance of PAR2$^{-/-}$ versus WT or PAR1$^{-/-}$, $P < 0.0001$, as determined with a log-rank test. *B,* PAR2$^{-/-}$ also showed delayed progression of multifocal disease, as quantified by the appearance of palpable tumors in each of the mammary glands. *C* and *D,* overall tumor burden was quantified by (*C*) tumor measurements with calipers using the formula volume = length × width^2/2 or (*D*) body weight. *Points,* mean; *bars,* SEM (*C*) or SD (*D*).

recapitulates important aspects of human breast cancer pathology (31). Our results document a crucial role for PAR2, but not PAR1, in breast cancer development and support the concept that PAR2 signaling is an upstream regulator of the angiogenic switch.

Materials and Methods

Mice. C57BL/6 PAR1$^{-/-}$ and PAR2$^{-/-}$ mice (13) were crossed with C57BL/6 MMTV-PyMT mice (32). PAR1$^{-/-}$ mice were backcrossed for 10 to 13 generations into the C57BL/6 background and PAR2$^{-/-}$/C57BL/6 founder lines were confirmed to be congenic with C57BL/6 by genome scanning. Wild-type (WT) PyMT controls were derived from the cross with the PAR2$^{-/-}$ strain. Cohorts of WT, PAR1$^{-/-}$, and PAR2$^{-/-}$ PyMT mice were followed by weekly palpation of all mammary glands for the appearance of tumors. Tumors were then measured in length and width with calipers for calculation of tumor volumes (length × width^2/2). Mice were sacrificed when the size of the largest tumor exceeded institutional guidelines, tumors and lungs were recovered, and macroscopic metastasis was determined by counting foci in fixed lungs. All animal experiments were performed under approved protocols of the Institutional Animal Care and Use Committee.

Real-time PCR. To determine lung metastasis, PyMT cDNA in lungs was detected by real-time PCR. In brief, mouse lungs were homogenized in 2.5 mL Trizol reagent and 1 mL homogenate was used for mRNA purification. cDNA was synthesized with SuperScript (Invitrogen) and 2 μg cDNA was used for the real-time PCR reaction using Taqman (Applied Biosystems). cDNA that was prepared from 3.5×10^6 WT PyMT cells was analyzed in parallel and the numbers of PyMT-positive cells in the lungs were then calculated based on the results obtained from the PyMT cell control. CXCL1 mRNA levels in PyMT cell lines were similarly determined by lysing the cells in 1 mL Trizol reagent after stimulation and generating cDNA as described above.

Western blot. PyMT cell lines were serum deprived for 24 h in DMEM, stimulated with 20 nmol/L thrombin, 100 μmol/L SLIGRL (PAR2 agonist), or 400 μmol/L AYPGKF (PAR4 agonist), and lysed in sample buffer. Extracellular signal-regulated kinase (ERK) phosphorylation was then determined by Western blotting with specific antibodies to mitogen-activated protein kinase (MAPK) ERK1/2 and phosphorylated ERK1/2 (Cell Signaling Technology).

Histology and immunohistochemistry. For whole-mount preparation of mammary glands, the fourth inguinal gland was removed and fixed in 4% paraformaldehyde for 2 h. Glands were stained overnight in Carmine red and then dehydrated in an alcohol bath. Glands were defatted with xylene overnight and mounted. For immunohistochemistry, the glands were fixed either in paraformaldehyde or in Zinc fixative and embedded in paraffin. Tissues were sectioned at 5 μm thickness, deparaffinized in xylene, rehydrated in a series of ethanol solutions, and directly incubated with blocking solution (Vector ABC Kit Elite). Tissues were incubated with primary antibodies diluted in blocking buffer for 2 h at room temperature or overnight at 4°C. Secondary antibodies coupled to biotin were incubated for 1 h at room temperature followed by the incubation for 30 min with ABC reagent. Horseradish peroxidase was developed in 3,3′-diaminobenzidine (Dako) chromogen according to the manufacturer's instructions, and tissues were counterstained with hematoxylin. Tissues were then dehydrated and mounted in Permount embedding medium.

Scoring of H&E-stained tumor sections was based on the description of four different stages by Lin and colleagues (33) and performed on numbered slides with unknown genotypes to the observer. Hyperplasia with intact basement membranes was defined by cuboidal cells with hyperchromatic nuclei and a reduced cytoplasmic to nuclear ratio. Adenomas were scored

based on differentiated and coalescing solid acinar arrangements that were locally invading, but the outline of the tumors was still well defined. Carcinomas were composed of cells with pleomorphic nuclei, but they had lost the basement membrane with the most aggressive stage characterized by large areas of poorly differentiated tumor cells. Tumor area was quantified with Photoshop CS2 and ImageJ.

Isolation of primary tumor cells from PyMT tumors. Primary PyMT tumor cells were obtained by mechanical dissociation of solid PyMT carcinomas and recovering outgrowth cells from plated tumor fragments. The tumor cells were grown in DMEM supplemented with 10% FCS and glutamine and tumor cell lines were established by passaging until cells with fibroblast-like appearance were eliminated from the cultures.

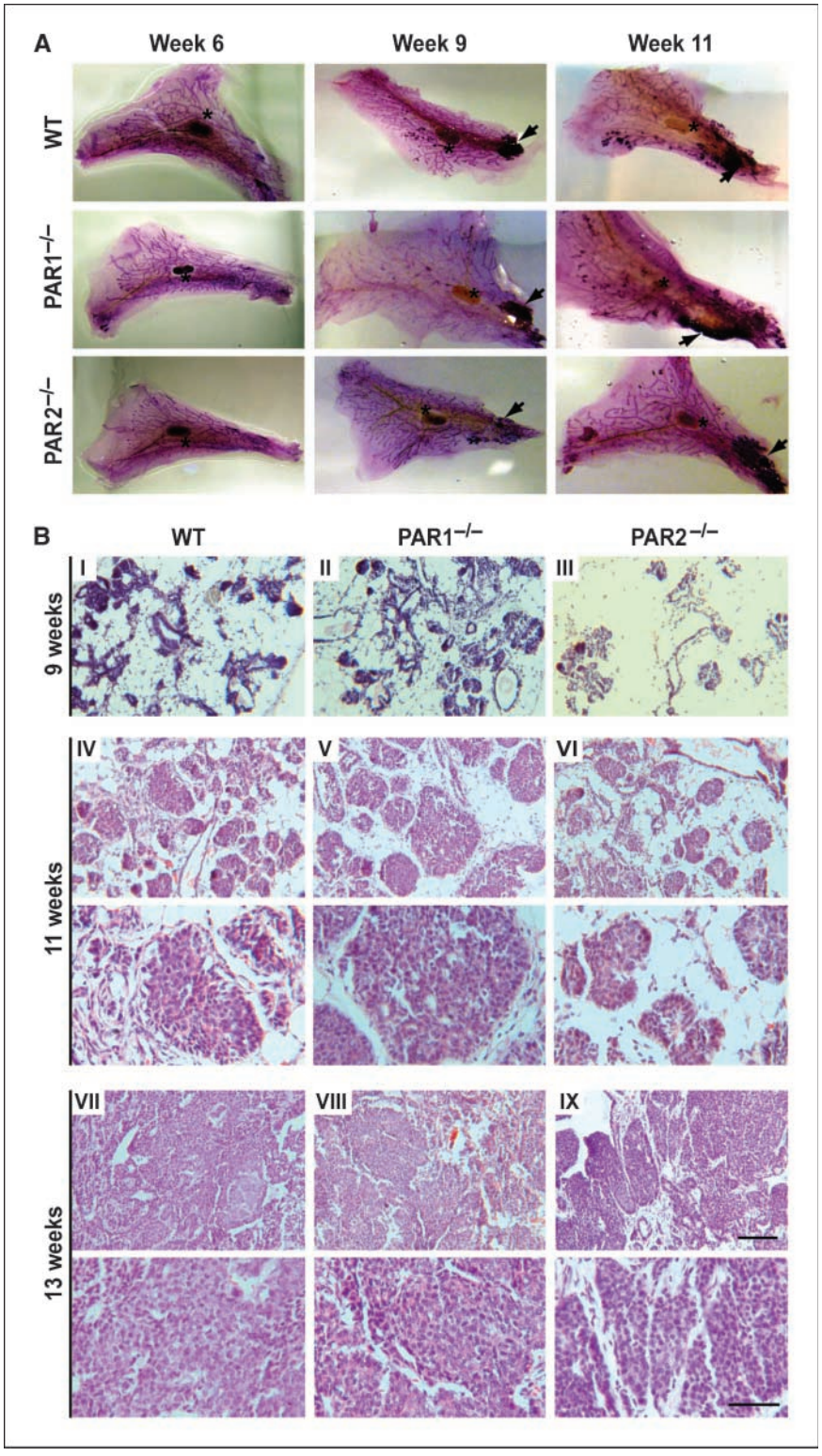

Figure 2. *A,* development of visible tumors in WT, PAR1$^{-/-}$, and PAR2$^{-/-}$ PyMT mice. Whole-mount analysis of mammary glands of virgin WT, PAR1$^{-/-}$, or PAR2$^{-/-}$ female mice at 6 wk of age show similar extension of breast architecture throughout the mammary fat. At 9 and 11 wk of age, primary tumors (*arrows*) are visible in all three genotypes, but tumor sizes are smaller in PAR2$^{-/-}$ PyMT mice. *, central lymph node. *B,* PAR2$^{-/-}$ PyMT mice display more benign tumors than WT and PAR1$^{-/-}$ PyMT mice in early stages of development. Tumors of 9-, 11-, and 13-wk-old mice were harvested, fixed, and stained with H&E. *I* to *III,* at 9 wk of age, the majority of the tumors consist of adenoma and hyperplasia lesions. At 11 wk, the majority of WT and PAR1$^{-/-}$ tumors are carcinomas (*IV, V*, and higher magnifications below), whereas the majority of PAR2$^{-/-}$ tumors are still at the stage of adenoma (*VI*). At 13 wk of age, most WT and PAR1$^{-/-}$ tumors and most PAR2$^{-/-}$ tumors are advanced carcinomas (*VII, VIII, IX*, and higher magnifications below). *IX, scale bar,* 100 μm (low-resolution pictures) and 50 μm (high-resolution pictures).

Table 1. Histologic features and tumor areas of WT, PAR1$^{-/-}$, and PAR2$^{-/-}$ PyMT tumors at 9 to 13 wk

	9-10 wk	11-12 wk	13 wk
WT			
Scoring	15% no tumor 24% hyperplasia 54% adenoma 7% carcinoma (N = 13, n = 12)	17% hyperplasia 8% adenoma 75% carcinoma (N = 13, n = 12)	25% adenoma 75% carcinoma (N = 8, n = 7)
Tumor area	38% (2 of 4)*	43% (3 of 10)	49% (4 of 8)
PAR1$^{-/-}$			
Scoring	11% hyperplasia 55% adenoma 34% carcinoma (N = 9, n = 8)	39% adenoma 61% carcinoma (N = 13, n = 12)	20% adenoma 80% carcinoma (N = 5, n = 5)
Tumor area	39% (4 of 8)	45% (4 of 13)	49% (2 of 5)
PAR2$^{-/-}$			
Scoring†	23% no tumor 31% hyperplasia 39% adenoma 7% carcinoma (N = 13, n = 13)	14% hyperplasia 58% adenoma 28% carcinoma (N = 7, n = 6)	33% adenoma 66% carcinoma (N = 9, n = 9)
Tumor area	30% (5 of 6)	38% (4 of 6)	44% (4 of 8)

Abbreviations: N, number of tumors scored; n, number of mice analyzed; no tumor, no tumor detectable on section.
* Number of tumors with tumor area smaller than average WT tumor area.
† χ^2 testing shows a different distribution of scored tumor categories for PAR2$^{-/-}$ and PAR1$^{-/-}$ mice at 9 to 10 wk (P = 0.016) and PAR2$^{-/-}$ and WT mice at 11 to 12 wk (P < 0.01). No statistically significant differences between PAR1$^{-/-}$ and WT at all times, PAR2$^{-/-}$ and WT at 9 to 10 wk, and PAR2$^{-/-}$ and PAR1$^{-/-}$ at 11 to 12 wk.

Tumor growth assay. PyMT-derived cells (2×10^7/mL) were injected s.c. in 100 μL PBS into the flank of WT or PAR2$^{-/-}$ mice. Tumors were measured twice weekly with calipers.

CXCL1 ELISA. Tumors from WT and PAR2$^{-/-}$ mice were harvested and homogenized in 30 mmol/L Tris (pH 7.4), 150 mmol/L NaCl, 1% Triton X-100, 2 mmol/L $CaCl_2$, 2 mmol/L $MgCl_2$, and protease inhibitor cocktail. Mammary fat pad from non-PyMT mice was taken as control. CXCL1 ELISA was performed on cleared extracts according to the manufacturer's protocol (R&D Systems) with normalization for protein concentration.

Statistical analysis. Differences in the appearance of palpable tumors were determined by log-rank test (Prism 4). Differences in histologic tumor scoring between WT, PAR1$^{-/-}$, and PAR2$^{-/-}$ cohorts were evaluated by a χ^2 testing for goodness of fit with two categories where one distribution (observed) is assumed to have come from the same population (expected) as a reference distribution. The χ^2 distribution is $\chi^2 = \sum_{i=1}^{k} \frac{(f_i - \hat{f}_i)^2}{\hat{f}_i}$, where f_i is the frequency observed in category i, $\hat{f}_i$ is the frequency expected in category i, and the summation is performed over all the categories k of the data. The probability is determined from a table of critical values for the χ^2 distribution using the calculated value of χ^2 and the degrees of freedom ($k - 1$, in this case 3). The two distributions are considered to be different when the P values are <0.05.

Results

PAR2, but not PAR1, is important for breast tumor development. To investigate the relative contributions of PAR1 and PAR2 to the development of breast cancer, we crossed PAR1$^{-/-}$ and PAR2$^{-/-}$ mice with the MMTV-PyMT tumor model in the C57BL/6 background. PyMT tumor development in the C57BL/6 background is significantly delayed compared with the more aggressive FVB background and the C57BL/6 strain facilitates the analysis of both accelerated and delayed tumor growth phenotypes (32). Cohorts of WT, PAR1$^{-/-}$, and PAR2$^{-/-}$ MMTV-PyMT mice were followed for the appearance of palpable tumors in each of the mammary glands, overall tumor burden, and changes in body weight. The appearance of palpable tumors was indistinguishable between WT and PAR1$^{-/-}$ mice but significantly delayed in PAR2-deficient animals (Fig. 1*A*). Multifocal disease was similarly delayed, as indicated by the number of mammary glands that developed palpable tumors over time (Fig. 1*B*). Importantly, tumor mass and overall body weight increases were indistinguishable between WT and PAR1$^{-/-}$ mice, excluding a specific role for PAR1 in tumor expansion, remodeling of the tumor microenvironment, or late-stage tumor cell survival (Fig. 1*C* and *D*). As expected from the delayed tumor onset, tumor burden and overall body weight were decreased in PAR2$^{-/-}$ mice (Fig. 1*C* and *D*). Together, these data show that PAR2, but not PAR1, is important for mammary tumor development in the PyMT model.

Delayed development of adenocarcinomas in PAR2$^{-/-}$ mice. The delayed appearance of palpable tumors in PAR2$^{-/-}$ PyMT mice may have been caused by abnormal mammary gland development. To rule out this possibility, whole mounts were prepared of the fourth inguinal mammary gland of virgin PAR2$^{-/-}$, PAR1$^{-/-}$, and WT mice at prepubertal (4 weeks) and pubertal (6 weeks) age. Budding from the primary ducts (4 weeks; data not shown) and expansion of mammary ducts to the entire fat pad (6 weeks) were similar in all three genotypes (Fig. 2*A*). Thus, the delay in the tumor

onset in PAR2$^{-/-}$ mice was not due to a defect in mammary gland development.

To address adenoma and early adenocarcinoma development in these mice, whole mounts of PyMT-positive fourth inguinal glands were analyzed at the age of 9 and 11 weeks. All WT, PAR1$^{-/-}$, and PAR2$^{-/-}$ mice had visible adenomas at 9 weeks, excluding that adenomas developed later in PAR2$^{-/-}$ mice (Fig. 2*A*). However, the sizes of visible tumors were consistently larger in WT and PAR1$^{-/-}$ relative to PAR2$^{-/-}$ mice. Eighty-three percent and 75% of primary tumors were >2 mm in diameter for WT (6 mice, 12 glands) and PAR1$^{-/-}$ mice (2 mice, 4 glands), respectively, versus 17% (3 mice, 6 glands) for PAR2$^{-/-}$ mice, indicating delayed tumor progression. Mammary duct thickness was quantified on whole mounts of 9- to 11-week-old mice as an independent measure for hyperplasia and adenoma formation. No differences were found between PAR1$^{-/-}$, PAR2$^{-/-}$, and WT mice (data not shown).

To further characterize the development of early carcinomas, tumors from 9- to 13-week-old mice were analyzed by histology. We distinguished early and late carcinoma from adenomas based on the recommendations for the classification of mouse mammary tumor pathology panel (33). Adenomas were characterized as acini filled with cells that retain a basement membrane; adenocarcinomas were composed of cells with cytologic atypia and sign of invasion into the stroma with the more advanced stage composed of poorly differentiated tumor cells where the acini structure has disappeared. Whereas WT and PAR1$^{-/-}$ mice showed hyperplasia, adenoma, and some early carcinoma at 9 to 10 weeks, PAR2$^{-/-}$ mice showed mainly hyperplasia and adenoma but typically no adenocarcinoma at this stage (Fig. 2*B*; Table 1). Accordingly, the ratio of tumor area versus normal tissue in WT and PAR1$^{-/-}$ tumors was ~38% compared with 30% for PAR2$^{-/-}$ tumors (Table 1). At 11 and 12 weeks, WT and PAR1$^{-/-}$ mice showed marked progression with increased incidence of carcinomas (>60%), whereas PAR2$^{-/-}$ tumors were predominantly at the stage of adenoma with few carcinoma (28%). At 13 weeks of age, 75% of WT tumors were at the carcinoma stage and in 25% adenomas were still present and the corresponding numbers were 80% and 20% for PAR1$^{-/-}$ mice. PAR2$^{-/-}$ mice also showed more advanced tumors at that stage, but adenomas were still predominant in one third of PAR2$^{-/-}$ tumors.

Delayed angiogenic switch in PAR2$^{-/-}$ breast tumors. Detection of disrupted basement membrane layers of PAR1$^{-/-}$ and WT acini was consistent with beginning invasive carcinoma,

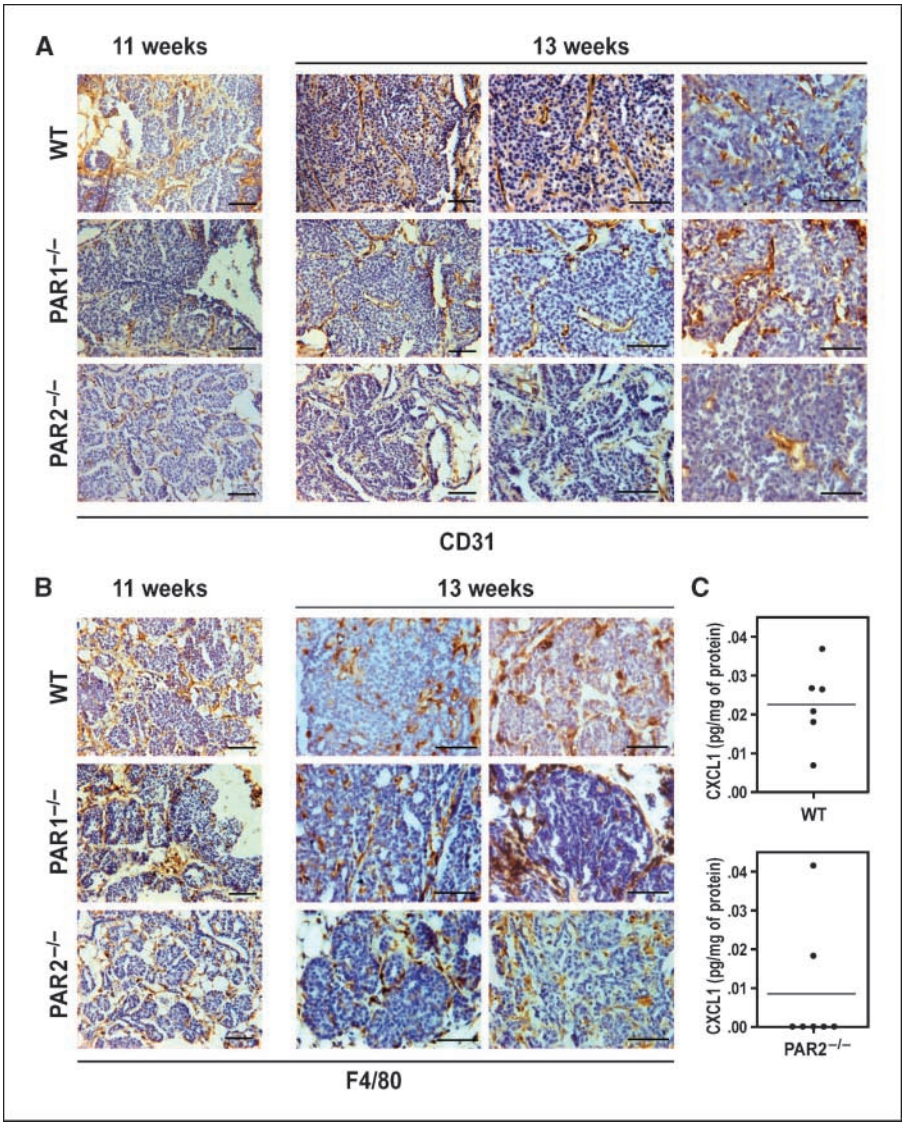

Figure 3. Delayed angiogenesis in PAR2$^{-/-}$ PyMT mice. *A* and *B*, tumors of 11- and 13-wk-old mice were stained for CD31 and F4/80 (*brown staining*). *A*, representative tumors at 11 and 13 wk are shown with low and higher magnification (*13 weeks, right two columns*). *B*, low-magnification (11 wk) and high-magnification (13 wk) images of representative F4/80 stainings. *Scale bars*, 50 μm. *C*, levels of CXCL1 were measured in tumor homogenates from 12-wk-old mice by ELISA. The bar represents the mean CXCL1 levels for each group. All WT, but only two of seven PAR2$^{-/-}$, tumors had detectable CXCL1 levels.

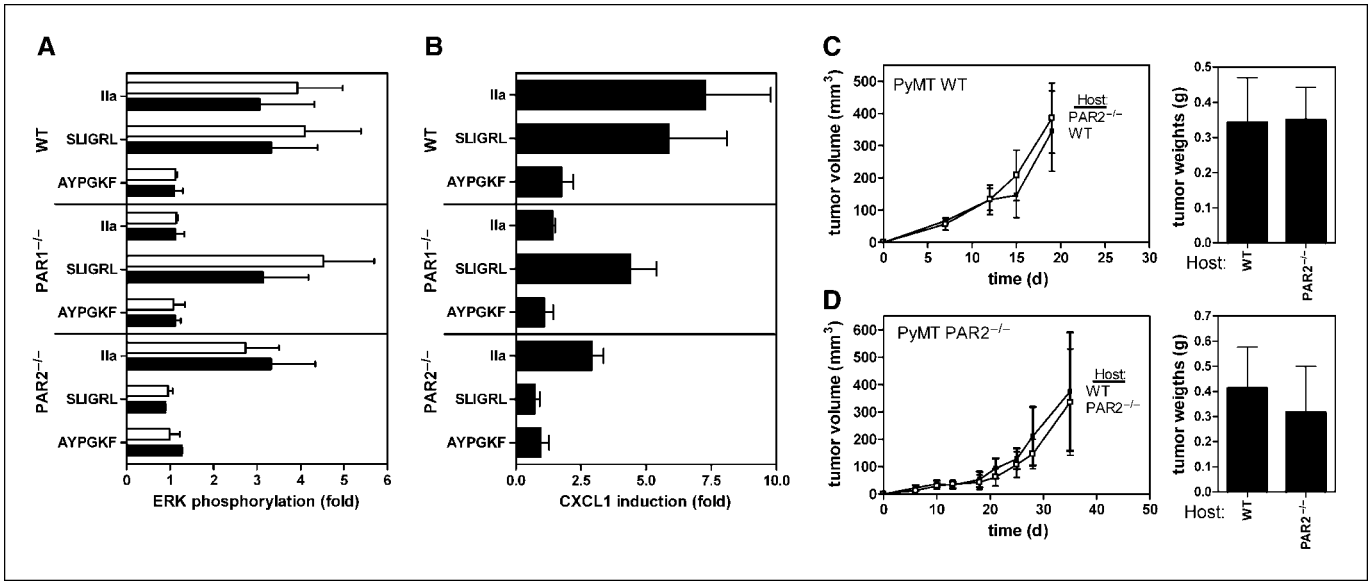

Figure 4. Characterization of PAR-deficient breast cancer cells. *A,* WT, PAR1$^{-/-}$, and PAR2$^{-/-}$ breast cancer cells were isolated from advanced tumors of two independent donor mice each (*black* and *white columns*). ERK1/2 phosphorylation following stimulation with 20 nmol/L thrombin (*IIa*), 100 μmol/L PAR2 agonist (*SLIGRL*), or 400 μmol/L PAR4 agonist (*AYPGKF*) was determined by Western blotting and quantified by densitometry ($n = 3$). *Columns,* mean; *bars,* SD. *B,* induction of CXCL1 mRNA by stimulation with the indicated agonists for 90 min was quantified by Taqman real-time PCR ($n = 3$). *Columns,* mean; *bars,* SD. *C* and *D,* tumor growth of WT (*C*) or PAR2$^{-/-}$ (*D*) breast cancer cells in syngeneic C57BL/6 WT or PAR2$^{-/-}$ mice. Cells (2×10^6) were injected s.c., tumor volumes were measured as indicated, and tumor weights were determined at sacrifice.

whereas acini structures remained frequently intact in PAR2$^{-/-}$ tumors even at 12 to 13 weeks. To provide insight whether the delayed tumor development in PAR2$^{-/-}$ was related to the angiogenic switch, tumors at 11 to 13 weeks were stained for CD31 to visualize vessels and F4/80 to detect angiogenesis-promoting tumor-associated macrophages (Fig. 3*A* and *B*). In 11-week-old WT and PAR1$^{-/-}$ mice, invading tumor vessels were already detectable, whereas CD31$^+$ vessels in PAR2$^{-/-}$ mice were mainly confined to areas that surrounded the tumor acini (Fig. 3*A*). At 13 weeks of age, WT and PAR1$^{-/-}$ tumors showed mainly well-vascularized carcinomas (Fig. 3*A*). In contrast, the stroma of PAR2$^{-/-}$ tumors showed fewer vessels compared with WT or PAR1$^{-/-}$ tumors (Fig. 3*A*). Recruitment of macrophages is an important determinant of tumor development and linked to the angiogenic switch in the PyMT model (34). F4/80$^+$ macrophages were located mainly around the tumor acini in apparent association with vessels of WT, PAR1$^{-/-}$, and PAR2$^{-/-}$ mice at 11 weeks (Fig. 3*B*). At 13 weeks, macrophages were detected throughout the stroma of WT and PAR1$^{-/-}$ tumors in a distribution that indicated invasion of the stroma, but macrophages also remained associated with tumor vessels. Similar to the reduced vessel density, staining for F4/80$^+$ seemed to be sparse in PAR2$^{-/-}$ relative to WT and PAR1$^{-/-}$ tumors.

Defects in angiogenesis can be caused by impaired tumor cell production of cytokines and/or chemokines. CXCL1 (KC, Gro-α) is a chemokine that is part of the metastasis and tumor growth–promoting signature of breast cancer cells (35) and has been linked to proangiogenic activities of thrombin signaling (36). Breast cancer cell PAR2 signaling induces a broad repertoire of angiogenic regulators, including CXCL1 (11). To address local, tumor-derived production of CXCL1, mammary tumors from 12-week-old mice were homogenized for CXCL1 determination by ELISA. All WT tumors had detectable levels of CXCL1, but only two of seven PAR2$^{-/-}$ tumors produced CXCL1 (Fig. 3*C*). These data indicated that PAR2 signaling regulates CXCL1 *in vivo*. CXCL1 may promote tumor progression in this model by regulating early tumor angiogenesis either directly or through the induction of other chemokines (36). Analysis of advanced tumors did not reveal any differences in morphology, microvessel density, or macrophage infiltration between genotypes (data not shown). These data are consistent with the concept that multiple proangiogenic pathways can drive tumor progression after the angiogenic switch has occurred and that alternative proangiogenic factors can compensate for the loss of PAR signaling.

PAR1 and PAR2 signaling contributes to CXCL1 induction in PyMT breast cancer cells. Because several PARs are activated by thrombin, it was important to address whether deletion of PAR1 abolished thrombin responsiveness of PyMT breast cancer cells. Cell lines were established from advanced WT, PAR1$^{-/-}$, and PAR2$^{-/-}$ tumors after mechanical dispersion and outgrowth from mixed cultures. We used MAPK ERK1/2 phosphorylation and CXCL1 induction as independent signaling readouts to characterize PAR signaling in these cells. WT breast cancer cells were responsive to thrombin and the PAR2 agonist SLIGRL but not the PAR4 agonist peptide AYPGKF (Fig. 4*A* and *B*). Deletion of PAR1 abolished thrombin signaling and no compensatory up-regulation of PAR4 signaling was apparent at the functional level. Conversely, PAR2$^{-/-}$ breast cancer cells retained thrombin signaling but lost PAR2 agonist peptide-induced ERK1/2 phosphorylation and CXCL1 induction. These data confirm the expected loss of proangiogenic PAR2 signaling in PAR2$^{-/-}$ cells and argue against the possibility that normal breast cancer development in PAR1$^{-/-}$ mice was due to compensatory up-regulation of PAR4-mediated thrombin signaling of tumor cells.

Our previous studies showed that transplanted syngeneic tumors grew indistinguishably in PAR1$^{-/-}$ or PAR2$^{-/-}$ hosts (13). Because host PAR2 can contribute to angiogenesis (37–39), we wanted to exclude the possibility that breast cancer cells specifically depend

on host PAR2 signaling. Experiments comparing the growth of transplanted PyMT tumor lines in WT and PAR2$^{-/-}$ mice (Fig. 4*C*) confirmed that PAR2 deficiency on host cells has no role in promoting s.c. breast cancer cell growth. In addition, growth of PAR2$^{-/-}$ tumor cells in WT versus PAR2$^{-/-}$ mice was indistinguishable, excluding that it is necessary to delete PAR2 on host and tumor cells to uncover a role for host PAR2 in tumor growth (Fig. 4*D*).

Spontaneous metastasis in the PyMT model. Metastasis was quantified at sacrifice of the cohort by two independent methods. One half of the lung was fixed for counts of macroscopic metastases, whereas the other half was analyzed by real-time PCR for mRNA expression of the PyMT transgene that is expressed by tumor cells but not normal lung tissue. There was no significant difference in lung metastasis between WT and PAR1$^{-/-}$ mice, both in the number of macroscopic metastases and total metastatic burden (Fig. 5*A* and *B*). Metastasis was reduced in age-matched PAR2$^{-/-}$ relative to WT mice. As expected, this subgroup had lower primary tumor burden and multifocal disease, and a shorter time from tumor appearance to tumor staging relative to WT (Fig. 5*C* and *D*). We also followed another subgroup of PAR2$^{-/-}$ mice for a longer time (Fig. 5*C*), which yielded tumor burden and duration of tumor growth similar to WT mice (Fig. 5*C* and *D*). Although medians for macroscopic metastasis and metastatic burden were reduced, this cohort was not statistically significantly different from WT mice. Thus, metastasis was primarily attenuated as a result of delayed tumor development in PAR2$^{-/-}$ mice.

Discussion

Here, we addressed the role of protease signaling in mammary tumor development and progression and show that PAR2, but not PAR1, deficiency leads to a delay in the appearance of palpable tumors and progression of multifocal disease in the PyMT model of breast cancer. The mammary glands developed normally and transgene-induced adenoma formation was not prevented in PAR2$^{-/-}$ mice. However, the progression to adenocarcinoma was delayed. Early-stage WT and PAR1$^{-/-}$ tumors attracted new blood vessels and showed indistinguishable progression to carcinomas. In contrast, PAR2$^{-/-}$ tumors showed reduced vessel infiltration and maintained the appearance of adenoma longer in comparison

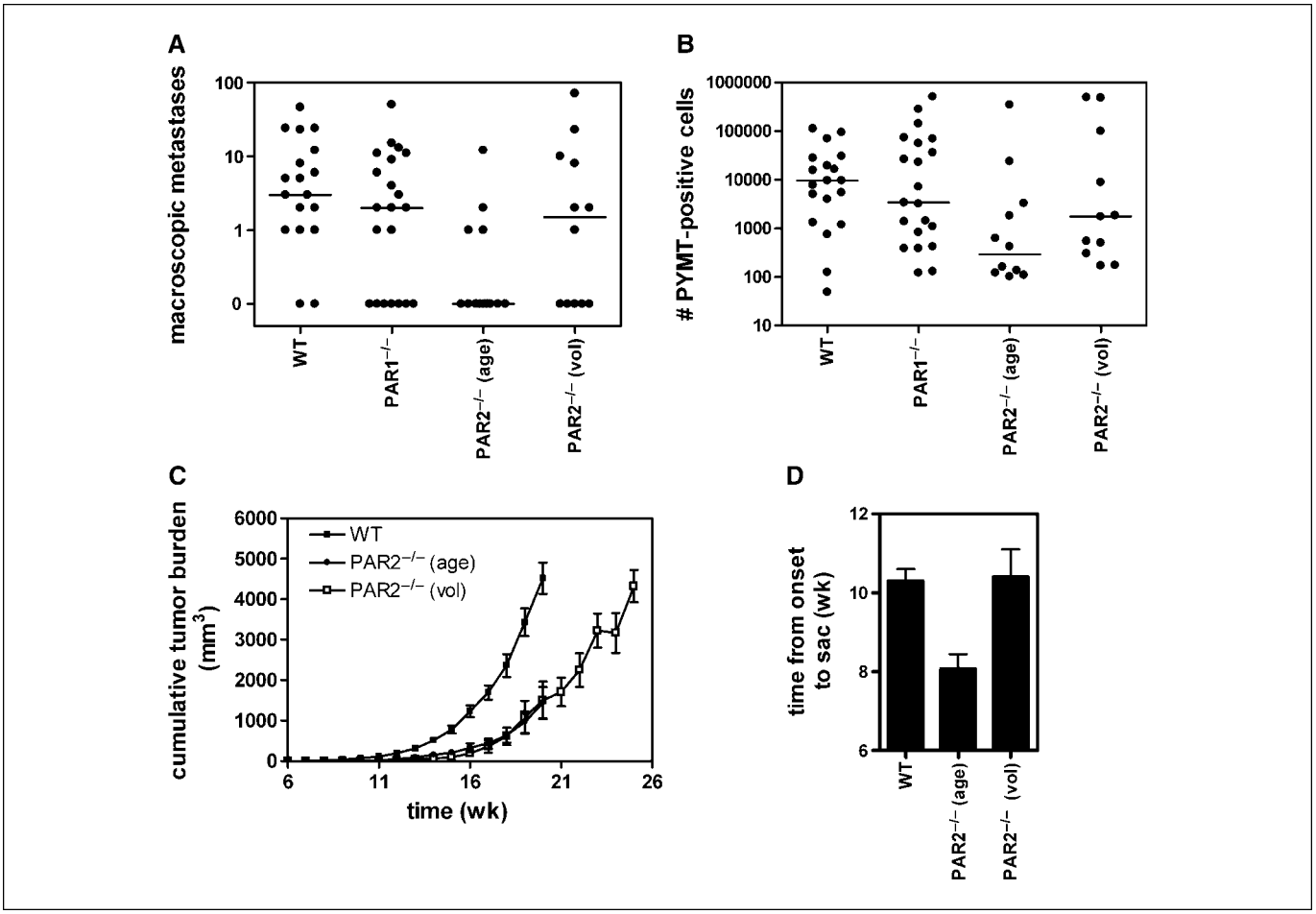

Figure 5. Spontaneous metastasis in WT, PAR1$^{-/-}$, and PAR2$^{-/-}$ PyMT mice. *A,* macroscopic metastases in WT, PAR1$^{-/-}$, and PAR2$^{-/-}$ PyMT mice. Mice were sacrificed at 20 wk of age or later for a subcohort of PAR2$^{-/-}$ mice, the lungs were extracted, and the numbers of visible metastases were counted. Subcohorts of PAR2$^{-/-}$ PyMT mice were grouped based on 20-wk average age (*age*) similar to WT or tumor burden (*vol*) that was comparable with WT and PAR1$^{-/-}$ mice. Medians are shown ($P = 0.329$ and 0.085 for PAR1$^{-/-}$ and volume-matched PAR2$^{-/-}$ versus WT; $P = 0.001$ for PAR2$^{-/-}$ age-matched versus WT, Mann-Whitney test). *B,* metastatic burden based on lung PyMT mRNA levels of WT, PAR1$^{-/-}$, and PAR2$^{-/-}$ PyMT mice. The number of PyMT-positive cells in age-matched PAR2$^{-/-}$ lungs ($P = 0.016$), but not in PAR1$^{-/-}$ ($P = 0.871$) or volume-matched PAR2$^{-/-}$ lungs ($P = 0.414$), was significantly different from WT. *C,* tumor burden in WT and PAR2$^{-/-}$ subcohorts. *D,* time from appearance of palpable tumors to sacrifice in WT and subgroups of PAR2$^{-/-}$ mice.

with WT or PAR1$^{-/-}$ tumors from mice of similar age. These data indicate that PAR2 signaling provides cues to initiate the angiogenic switch.

The normal progression of tumor development in PAR1$^{-/-}$ mice was surprising, considering the documented roles of PAR1 signaling and thrombin in angiogenesis and breast cancer cell motility (9, 22–24, 29). We found no compensatory up-regulation of alternative thrombin receptors on PAR1$^{-/-}$ PyMT tumor cells and our results are in concordance with previous studies that did not uncovered an essential role for host PAR1 in the growth of tumors or metastases (13, 14). The lack of an appreciable phenotype of PAR1$^{-/-}$ PyMT mice suggests that PAR1 signaling on both tumor or host cells is not required to modulate mammary tumor progression in this model in C57BL/6 mice. Although no strict comparison has been performed in tumor models, there is no experimental evidence that mouse PAR1 and PAR2 have roles that are fundamentally different from the human counterparts. However, mouse platelets are activated independent of PAR1 and our mouse studies are entirely consistent with previously documented roles of platelet thrombin signaling in tumor biology.

A considerable body of data also documents a role for tumor cell PAR1 signaling in metastasis (26), but spontaneous metastasis in PyMT PAR1$^{-/-}$ mice seemed to be indistinguishable from WT PyMT mice. Delayed tumor development led to decreased metastasis in PAR2$^{-/-}$ mice. However, there was no statistically significant reduction of metastasis in PAR2$^{-/-}$ mice when a subgroup with similar tumor burden was compared with WT. Because both PAR1 and PAR2 can contribute to metastasis (26, 40), partial compensation by the other PAR and the high variability of spontaneous metastasis in the PyMT model may have obscured the previously documented roles of PARs in metastatic disease. In addition, experimental metastasis assays are also expected to have higher sensitivity to specifically detect tumor cell phenotypes in the various stages of metastatic homing to the lung.

Macrophage recruitment and vessel density were similarly reduced in early PAR2$^{-/-}$ tumors. The angiogenic switch and progression of the PyMT breast cancer model is closely correlated with macrophage infiltration of early tumors (33, 34). Colony-stimulating factor (CSF) 1 (macrophage CSF) is the key tumor cell–derived chemoattractant for the recruitment of macrophages, which in turn enables angiogenesis-dependent tumor cell intravasation and metastasis. Breast cancer cell PAR2 signaling induces the synthesis of CSF1 and other chemokines, such as granulocyte macrophage CSF2, IL-8, and CXCL1 (11), which may promote angiogenesis directly (CXCL1; ref. 36) or indirectly (CSF1) through macrophage recruitment. CXCL1 has frequently been implicated in tumor angiogenesis in various cancers, including melanoma and breast (41, 42). CXCL1 levels were reduced in early PAR2$^{-/-}$ tumors, suggesting a link between PAR2 signaling and early pro-angiogenic chemokine production in breast cancer progression.

Several proteases, including trypsin, factor Xa, and matriptase, are known to activate PAR2 on cancer cells (10, 19, 43). TF expression in clinical breast cancer (44) and several lines of experimental evidence implicate the TF-VIIa complex as a relevant PAR2 activator in breast cancer. TF-VIIa induces efficiently the repertoire of PAR2-responsive genes (11) and promotes breast cancer cell motility (12, 19). We have recently identified a monoclonal antibody to TF that specifically blocks TF-VIIa signaling but not coagulation. Orthotopic growth of breast cancer xenografts and local angiogenesis were significantly attenuated by specific blockade of TF-dependent PAR2 signaling using this antibody that targets tumor cell TF (18). TF-VIIa may play this unique role in promoting the angiogenic switch because tumor cells respond to hypoxia with the up-regulation of the ligand of TF, VIIa (16), which enables coagulation protease signaling in the extravascular space. Indeed, elimination of the response to hypoxia by hypoxia-inducible factor 1α deletion in breast cancer cells produces a delay of PyMT tumor development that is remarkably similar to the phenotype of PAR2$^{-/-}$ mice (45).

In this present study, one cannot completely rule out the possibility that the delayed angiogenic switch is indirectly caused by a decreased cell mass of the developing adenomas. Indeed, TF-VIIa-PAR2 signaling has been implicated in the regulation of tumor cell migration, proliferation, and apoptosis (12, 19, 20, 46, 47). However, it is unlikely that PAR2 is a major contributor to tumor cell proliferation because tumor expansion was normal once the angiogenic switch occurred in PAR2$^{-/-}$ mice. These data further indicate that inhibition of PAR2 signaling is not a strategy for direct antitumor therapy. Rather, targeting PAR2 is more likely beneficial in the context of conventional cytostatic therapies by inducing tumor dormancy through blockade of a tumor cell–initiated proangiogenic program.

Disclosure of Potential Conflicts of Interest

No potential conflicts of interest were disclosed.

Acknowledgments

Received 2/4/2008; revised 5/30/2008; accepted 6/29/2008.

Grant support: NIH grants HL60742 and HL16411 (W. Ruf) and K22CA118182 (L.G. Ellies), California Breast Cancer Research Project postdoctoral fellowship 13FB-0125 (F. Schaffner), and Netherlands Scientific Organization grant S92-251 (H.H. Versteeg).

The costs of publication of this article were defrayed in part by the payment of page charges. This article must therefore be hereby marked *advertisement* in accordance with 18 U.S.C. Section 1734 solely to indicate this fact.

We thank Jennifer Royce, Ngan Pham-Mitchell, Pablito Tejada, Rahel Delears, and Cindi Biazak for assistance and Lana Schaffer for statistical analysis.

References

1. Rickles FR, Patierno S, Fernandez PM. Tissue factor, thrombin, and cancer. Chest 2003;124:58–68S.
2. Schulman S, Lindmarker P. Incidence of cancer after prophylaxis with warfarin against recurrent venous thromboembolism. Duration of Anticoagulation Trial. N Engl J Med 2000;342:1953–8.
3. Belting M, Ahamed J, Ruf W. Signaling of the tissue factor coagulation pathway in angiogenesis and cancer. Arterioscler Thromb Vasc Biol 2005;25:1545–50.
4. Zhang Y, Deng Y, Luther T, et al. Tissue factor controls the balance of angiogenic and antiangiogenic properties of tumor cells in mice. J Clin Invest 1994;94:1320–7.
5. Kakkar AK, Chinswangwatanakul V, Lemoine NR, Tebbutt S, Williamson RCN. Role of tissue factor expression on tumour cell invasion and growth of experimental pancreatic adenocarcinoma. Br J Surg 1999;86:890–4.
6. Abe K, Shoji M, Chen J, et al. Regulation of vascular endothelial growth factor production and angiogenesis by the cytoplasmic tail of tissue factor. Proc Natl Acad Sci U S A 1999;96:8663–8.
7. Yu JL, May L, Lhotak V, et al. Oncogenic events regulate tissue factor expression in colorectal cancer cells: implications for tumor progression and angiogenesis. Blood 2005;105:1734–41.
8. Palumbo JS, Talmage KE, Massari JV, et al. Tumor cell-associated tissue factor and circulating hemostatic factors cooperate to increase metastatic potential through natural killer cell-dependent and -independent mechanisms. Blood 2007;110:133–41.
9. Nierodzik ML, Karpatkin S. Thrombin induces tumor growth, metastasis, and angiogenesis: evidence for a thrombin-regulated dormant tumor phenotype. Cancer Cell 2006;10:355–62.
10. Ruf W, Mueller BM. Thrombin generation and the pathogenesis of cancer. Semin Thromb Hemost 2006;32 Suppl 1:61–8.
11. Albrektsen T, Sorensen BB, Hjortoe GM, Fleckner J, Rao LVM, Petersen LC. Transcriptional program induced by factor VIIa-tissue factor, PAR1 and PAR2

in MDA-MB-231 cells. J Thromb Haemost 2007;5:1588–97.
12. Hjortoe GM, Petersen LC, Albrektsen T, et al. Tissue factor-factor VIIa specific up-regulation of IL-8 expression in MDA-MB-231 cells is mediated via PAR-2 and results in increased cell migration. Blood 2004;103:3029–37.
13. Uusitalo-Jarvinen H, Kurokawa T, Mueller BM, Andrade-Gordon P, Friedlander M, Ruf W. Role of protease activated receptor 1 and 2 signaling in hypoxia-induced angiogenesis. Arterioscler Thromb Vasc Biol 2007;27:1456–62.
14. Camerer E, Qazi AA, Duong DN, Cornelissen I, Advincula R, Coughlin SR. Platelets, protease-activated receptors, and fibrinogen in hematogenous metastasis. Blood 2004;104:397–401.
15. Ahamed J, Versteeg HH, Kerver M, et al. Disulfide isomerization switches tissue factor from coagulation to cell signaling. Proc Natl Acad Sci U S A 2006;103:13932–7.
16. Koizume S, Jin M-S, Miyagi E, et al. Activation of cancer cell migration and invasion by ectopic synthesis of coagulation factor VII. Cancer Res 2006;66:9453–60.
17. Dorfleutner A, Hintermann E, Tarui T, Takada Y, Ruf W. Crosstalk of integrin α3β1 and tissue factor in cell migration. Mol Biol Cell 2004;15:4416–25.
18. Versteeg HH, Schaffner F, Kerver M, et al. Inhibition of tissue factor signaling suppresses tumor growth. Blood 2008;111:190–9.
19. Morris DR, Ding Y, Ricks TK, Gullapalli A, Wolfe BL, Trejo J. Protease-activated receptor-2 is essential for factor VIIa and Xa-induced signaling, migration, and invasion of breast cancer cells. Cancer Res 2006;66:307–14.
20. Zoudilova M, Kumar P, Ge L, Wang P, Bokoch GM, DeFea KA. β-Arrestin-dependent regulation of the cofilin pathway downstream of protease-activated receptor-2. J Biol Chem 2007;282:20634–46.
21. Kamath L, Meydani A, Foss F, Kuliopulos A. Signaling from protease-activated receptor-1 inhibits migration and invasion of breast cancer cells. Cancer Res 2001;61:5933–40.
22. Boire A, Covic L, Agarwal A, Jacques S, Sherifi S, Kuliopulos A. PAR1 is a matrix metalloprotease-1 receptor that promotes invasion and tumorigenesis of breast cancer cells. Cell 2005;120:303–13.
23. Even-Ram S, Uziely B, Cohen P, et al. Thrombin receptor overexpression in malignant and physiological invasion processes. Nat Med 1998;4:909–14.
24. Even-Ram SC, Maoz M, Pokroy E, et al. Tumor cell invasion is promoted by activation of protease activated receptor-1 in cooperation with the αvβ5 integrin. J Biol Chem 2001;276:10952–62.
25. Yin YJ, Salah Z, Grisaru-Granovsky S, et al. Human protease-activated receptor 1 expression in malignant epithelia. A role in invasiveness. Arterioscler Thromb Vasc Biol 2003;23:940–4.
26. Nierodzik ML, Chen K, Takeshita K, et al. Protease-activated receptor 1 (PAR-1) is required and rate-limiting for thrombin-enhanced experimental pulmonary metastasis. Blood 1998;92:3694–700.
27. Martin CB, Mahon G, Klinger M, et al. The thrombin receptor, PAR-1, causes transformation by activation of Rho-mediated signaling pathways. Oncogene 2001;20:1953–63.
28. Yin YJ, Katz V, Salah Z, et al. Mammary gland tissue targeted overexpression of human protease-activated receptor 1 reveals a novel link to β-catenin stabilization. Cancer Res 2006;66:5224–33.
29. Yin YJ, Salah Z, Maoz M, et al. Oncogenic transformation induces tumor angiogenesis: a role for PAR1 activation. FASEB J 2003;17:163–74.
30. Guy CT, Cardiff RD, Muller WJ. Induction of mammary tumors by expression of polyomavirus middle T oncogene: a transgenic mouse model for metastatic disease. Mol Cell Biol 1992;12:954–61.
31. Lin EY, Jones JG, Li P, et al. Progression to malignancy in the polyoma middle T oncoprotein mouse breast cancer model provides a reliable model for human diseases. Am J Pathol 2003;163:2113–26.
32. Davie SA, Maglione JE, Manner CK, et al. Effects of FVB/NJ and C57Bl/6J strain backgrounds on mammary tumor phenotype in inducible nitric oxide synthase deficient mice. Transgenic Res 2007;16:193–201.
33. Lin EY, Nguyen AV, Russell RG, Pollard JW. Colony-stimulating factor 1 promotes progression of mammary tumors to malignancy. J Exp Med 2001;193:727–40.
34. Lin EY, Li JF, Gnatovskiy L, et al. Macrophages regulate the angiogenic switch in a mouse model of breast cancer. Cancer Res 2006;66:11238–46.
35. Minn AJ, Gupta GP, Siegel PM, et al. Genes that mediate breast cancer metastasis to lung. Nature 2005;436:518–24.
36. Caunt M, Hu L, Tang T, Brooks PC, Ibrahim S, Karpatkin S. Growth-regulated oncogene is pivotal in thrombin-induced angiogenesis. Cancer Res 2006;15;66:4125–32.
37. Belting M, Dorrell MI, Sandgren S, et al. Regulation of angiogenesis by tissue factor cytoplasmic domain signaling. Nat Med 2004;10:502–9.
38. Zhu T, Sennlaub F, Beauchamp MH, et al. Proangiogenic Effects of Protease-Activated Receptor 2 Are Tumor Necrosis Factor-{α} and Consecutively Tie2 Dependent. Arterioscler Thromb Vasc Biol 2006;26:744–50.
39. Milia AF, Salis MB, Stacca T, et al. Protease-activated receptor-2 stimulates angiogenesis and accelerates hemodynamic recovery in a mouse model of hindlimb ischemia. Circ Res 2002;91:346–52.
40. Shi X, Gangadharan B, Brass LF, Ruf W, Mueller BM. Protease-activated receptor 1 (PAR1) and PAR2 contribute to tumor cell motility and metastasis. Mol Cancer Res 2004;2:395–402.
41. Kluger HM, Chelouche LD, Kluger Y, et al. Using a xenograft model of human breast cancer metastasis to find genes associated with clinically aggressive disease. Cancer Res 2005;65:5578–87.
42. Owen JD, Strieter R, Burdick M, et al. Enhanced tumor-forming capacity for immortalized melanocytes expressing melanoma growth stimulatory activity/growth-regulated cytokine β and γ proteins. Int J Cancer 1997;73:94–103.
43. Takeuchi T, Harris JL, Huang W, Yan KW, Coughlin SR, Craik CS. Cellular localization of membrane-type serine protease 1 and identification of protease-activated receptor-2 and single-chain urokinase-type plasminogen activator as substrates. J Biol Chem 2000;275:26333–42.
44. Sturm U, Luther T, Albrecht S, Flössel C, Grossmann H, Müller M. Immunohistological detection of tissue factor in normal and abnormal human mammary glands using monoclonal antibodies. Virchows Arch A Pathol Anat Hispathol 1992;421:79–86.
45. Liao D, Corle C, Seagroves TN, Johnson RS. Hypoxia-inducible factor-1α is a key regulator of metastasis in a transgenic model of cancer initiation and progression. Cancer Res 2007;67:563–72.
46. Sorensen BB, Rao LVM, Tornehave D, Gammeltoft S, Petersen LC. Anti-apoptotic effect of coagulation factor VIIa. Blood 2003;102:1708–15.
47. Versteeg HH, Spek CA, Richel DJ, Peppelenbosch MP. Coagulation factors VIIa and Xa inhibit apoptosis and anoikis. Oncogene 2004;23:410–7.